Fuel 313 (2022) 122981

Contents lists available at ScienceDirect

Fuel

journal homepage: www.elsevier.com/locate/fuel

Full Length Article

Direct conversion of syngas to ethanol over Rh-based and Cu-based tandem catalyst: Effect of Cu crystal plane

Yang Feng [a,b,c], Jungang Wang [c], Lixia Ling [a,d], Bo Hou [c], Riguang Zhang [a,b], Debao Li [c,*], Baojun Wang [a,b,*]

[a] State Key Laboratory of Clean and Efficient Coal Utilization, Taiyuan University of Technology, Taiyuan 030024, Shanxi, PR China
[b] Key Laboratory of Coal Science and Technology (Taiyuan University of Technology), Ministry of Education, Shanxi, PR China
[c] State Key Laboratory of Coal Conversion, Institute of Coal Chemistry, Chinese Academy of Sciences, Taiyuan 030001, Shanxi, PR China
[d] College of Chemistry and Chemical Engineering, Taiyuan University of Technology, Taiyuan 030024, Shanxi, PR China

ARTICLE INFO

Keywords:
Ethanol synthesis
Tandem catalyst
Crystal-plane
Rh-based catalyst
Cu_2O nanocrystals

ABSTRACT

Ethanol direct synthesis from CO hydrogenation over a tandem system composed of Rh/P25 and different facet Cu_2O nanocrystals are explored. The effect of Cu crystal plane is hindered by the complexity of the ethanol synthesis from syngas and the lack of adequate crystal plane structure data. In this work, the tandem catalysts Rh/P25 and the crystal-plane-controlled Cu_2O (cubes, octahedral Cu_2O, and 18 facet nanocrystals) are used to catalyze syngas to ethanol, in which 18 facet Cu_2O exposing {1 0 0}&{1 1 0} crystal planes is the more selective and catalytic activity for ethanol than Cu_2O cubes {1 0 0} and Cu_2O octahedral {1 1 1} crystal planes. The tandem system consisting of Rh/P25 and 18 facet Cu_2O NCs can afford the best catalytic activity (43.4%) and an ethanol selectivity of 18.7%. It is demonstrated that the selectivity and activity of the ethanol synthesis from syngas can be enhanced by tandem catalyst Rh-based and the selective exposure of Cu_2O nanocrystals with specific crystal planes. These results reveal that the selective exposure of Cu_2O nanocrystals with specific crystal planes is very helpful for enhancing the catalytic performance using tandem reaction of Rh-based and Cu NCs catalysts for ethanol synthesis from synthesis gas.

1. Introduction

Syngas (H_2 + CO) can be obtained from natural gas, coal and biomass, which is the most significant raw materials for chemical feedstocks and energy [1]. The chemical synthesis of ethanol from C1 resources via syngas is the hopeful methods. However, the development of efficient and optional catalysts for ethanol synthesis has been a major challenge. So far, there are four kind of catalysts that have been discussed for the direct synthesis of ethanol (EtOH) from carbon monoxide hydrogenation, that is Rh-based catalysts [2,3], modified Fischer–-Tropsch synthesis (FTS) catalysts [4,5], modified Cu-based catalysts [6,7] and Mo-based catalysts [8,9]. In recent years, Rh-based catalysts have been extensive and intensive research due to its excellent carbon chain growth ability. Rh-based is reported to be a good candidate for ethanol synthesis from carbon monoxide hydrogenation. Moreover, metals can be added as a promoter, which can significantly increase CO conversion and the selectivity of target products. Although the synthesis of EtOH has been made substantial progress, the process still faces major challenges in improving the alcohol selectivity, activity and long-term stability [10].

Anderson et al. [11] and Gonzalez et al. [12] claimed that copper poisons the catalytic activity to a large extent, and primarily suggestions mainly involve Rh sites on Cu-Rh/SiO_2 catalysts. In order to avoid copper poisoning the catalytic activity of Rh-based catalyst, a tandem catalyst in a dual-catalyst bed reactor can be adopted. Tandem catalysis, which can carry out multi-step sequential chemical reactions in a single fixed-bed reactor, has provided an opportunity to discover novel and more efficient catalytic processes [13,14]. Wang et al. [15,16] claimed that the reaction path can be adjusted by tandem catalysts to gain the desired chemical materials. Tandem catalysis can be a valid and practical way for further transformation of intermediates [17,18]. Recently, ethanol synthesis from syngas beyond Rh-based synthesis has recently been realized by designing dual-functional catalysts to CO hydrogenation to intermediate or ethanol and conversion of intermediate to

* Corresponding authors at: State Key Laboratory of Clean and Efficient Coal Utilization, Taiyuan University of Technology, Taiyuan 030024, Shanxi, PR China (B. Wang).
E-mail addresses: dbli@sxicc.ac.cn (D. Li), wangbaojun@tyut.edu.cn (B. Wang).

https://doi.org/10.1016/j.fuel.2021.122981
Received 26 October 2021; Received in revised form 3 December 2021; Accepted 14 December 2021
Available online 30 December 2021

desired product [19,20]. Very surprisingly, the tandem catalysis as described above could be synergistically enhanced [21,22]. However, it is noteworthy that the challenge of tandem catalysis is not only the adjustment of the mass ratio and proximity of these active components, but also the selection of active components and the control of its own hydrogenation capacity [23]. The development and research of a variety of routes to conversion of carbon monoxide hydrogenation to ethanol with high selectivity in a single-pass is very attractive but also extremely challenging.

Therefore, considering that syngas to ethanol occurred at a similar temperature for the Rh-based and Cu NCs catalysts, a twostep route to conversion of synthesis gas to ethanol using the tandem catalysts is proposed. However, the different crystal facets of the Cu-based catalyst have a great influence on the product selectivity and catalytic activity for ethanol synthesis from CO hydrogenation. Thus, we designed a series of tandem reactions to correlate product selectivity and the intrinsic catalytic activity with the corresponding crystal planes. It can be found that metallic nanoparticles (such as Cu-based catalyst) with low-index planes bonded by the substrate plane, that is, nanocube revealed {1 0 0} crystal plane, octahedra revealed {1 1 1} crystal plane and rhombic dodecahedra revealed {1 1 0} crystal plane [24]. Cu-based catalysts have been widely researched owing to its low cost, flexibility in structure control, simplicity to prepare and stabilization in performance, but the main product is methanol on the Cu-based catalysts. More and more density functional theory (DFT) calculations are used to comprehend the influence of the crystal plane on the catalytic activity and selectivity of the Cu NCs catalysts. Previously, our research group discovered that the mechanism and possible pathways for the formation of ethanol from CO hydrogenation on Cu(1 1 1), Cu(1 1 0) and Cu(1 0 0) surfaces by DFT calculations [25,26]. However, due to the structural sensitivity of the copper catalysts and its particularly susceptible to oxidation, which makes it hard for metallic copper to exist. The crystal plane effect of Cu-based catalyst is still a key challenge in the research to synthesize ethanol from syngas. The Cu-based catalyst without supports and additives has poor catalytic performance, and the crystal face effect of syngas to ethanol is not clear. Therefore, in order to optimize their catalysis activity, it is essential to control the exposed metal facets.

In this work, the design of a novel tandem catalytic systems for EtOH synthesis from syngas is reported. We discovered that the integration of Rh/P25 catalyst and different facets Cu NCs in tandem can afford syngas into ethanol with a selectivity of 18.7%. We illustrated that the careful design of different facet Cu NCs are vital to ethanol selectivity in the tandem catalytic systems. This work evaluates in detail the catalytic capability of tandem catalysts for EtOH synthesis and compares them with the physical mixed catalysts in order to find an ethanol synthesis catalyst with the best catalytic performance. Tandem catalyst Rh-based and Cu NCs with the crystal plane dependent catalytic function for the ethanol synthesis from syngas were explored and revealed.

2. Experimental section

2.1. Synthesis of catalysts

2.1.1. Synthesis of cubic Cu_2O nanocrystals

The synthesis of cubic Cu_2O NCs (c-Cu_2O) follows the procedures [27,28]: 100.0 mL sodium hydroxide aqueous solution (80.0 g/L) with a peristaltic pump is added dropwise into 1000 mL copper chloride aqueous solution (4.0 g/L) at 55 °C. After fully stirring for 30 min, 100.0 mL of ascorbic acid aqueous solution (105.7 g/L) with is added dropwise to the solution with a peristaltic pump. The mixed solution is thoroughly stirred 5 h at 55 °C. The resulting precipitate is collected by centrifugation, then wash several times with distilled water and absolute ethanol, and finally dried at 60 °C for 12 h in vacuum.

2.1.2. Synthesis of octahedral Cu_2O nanocrystals

Polyhedral octahedral Cu_2O NCs [29] were synthesized based on a representative procedure: copper acetate (6.0 g) was dissolved in H_2O (100 mL) and keep stirring at 70 °C for 2 min. When NaOH solution (7.2 g, 60 mL H_2O) is added dropwise to the above solution, precipitation will occur. After the above solution was stirred for 5 min, D-(+)-glucose powder (1.2 g) was added into the solution, and keep stirring for another 20 min at 70 °C. These precipitate-containing solutions were separated by centrifugation and washed with deionized water and ethanol for several times until the solution was neutral. Finally, the resulting precipitate was dried in a vacuum oven at 60 °C for 12 h.

2.1.3. Synthesis of 18 facet-Cu_2O nanocrystals

The synthesis of 18 facet Cu_2O nanocrystals (18-Cu_2O) followed the c-Cu_2O synthesis procedure. The difference is the concentration of $CuCl_2$ aqueous solution (8.0 g/L). In addition, other procedures are the same as the synthesis of c-Cu_2O.

2.1.4. Synthesis of Rh/P25 catalyst

The supported Rh catalyst is synthesized by incipient wetness impregnation. 10% rhodium nitrate solution (Aladdin) is used as the precursor of rhodium for catalyst. The Rh/P25 catalyst is prepared by dissolving 0.5 g 10% rhodium nitrate solution in 8 mL of ethanol and adding 5.0 g of P25 (Nano-TiO_2, Degussa AGTego) to this solution with constant stirring to the point of incipient wetness. The paste was incipient 24 h at room temperature in air, then the paste was dried 12 h in vacuum drying oven at 120 °C and subsequently calcined at 350 °C for 4 h in a muffle furnace. The catalyst was denoted as xRh/P25, where x represents the weight fraction of the element. The Rh weight in xRh/P25 catalyst is 0.86%, which determined by Inductively Coupled Plasma Optical Emission Spectrometry (ICP-OES) measurement.

2.1.5. Synthesis of Cu NCs

Various forms of Cu NCs are synthesized by the form retention reduction method [30]. The Cu_2O NCs (200 mg) is placed in a quartz tube and equilibrate with 5% CO/Ar for 30 min at room temperature, and then heated to 300 °C and reduced for 2 h, and finally cooled to room temperature. The obtained nanocube, octahedral and 18 facet Cu NCs are named c-Cu, o-Cu and 18-Cu, respectively.

2.2. Characterization techniques

Scanning electron microscope (SEM) (JSM-7001F) and a transmission electron microscope (TEM) (JEM-2100F) with an energy dispersive spectroscopy (EDS) are used. Powder X-ray diffraction (XRD) (PANalytical EmpyreanX'pert) uses monochromated Cu Kα radiation with the scan ranged from 5 to 90°. CO adsorption are obtained using a Fourier transform infrared (FT-IR) spectra (Thermo Scientific Nicolet 6700 spectrometer). The specific surface areas (BET) of the three types of Cu_2O and Rh/P25 catalyst are measured by N_2 adsorption method. X-ray photoelectron spectra (XPS) are carried out an AXIS ULTRA DLD instrument equipped.

H_2 temperature-programmed reduction (H_2-TPR) is carried out using a TP-5080 multipurpose automatic adsorption instrument. The sample (30 mg) is initially filled with Ar at 60 °C for 30 min. Next, a 10 vol% H_2/Ar mixture is flowed in (50 mL min^{-1}), and the temperature is increased to 900 °C at a heating slope of 10 °C min^{-1}.

The H_2-TPR profiles of the Rh/P25 and Cu_2O composites, the 30 mg Rh/P25 catalyst sample is placed on the upper layer of the U-shaped tube, and the 30 mg Cu_2O catalyst is placed on the lower layer of the U-shaped tube to simulate the sample loading method of the fixed bed reactor. The restoration procedure is the same as above.

2.3. Catalytic evaluation

The evaluation of the catalysts is carried out using the stainless steel fixed bed reactor. First, the catalyst (0.5 g powder, 40–60 mesh) is reduced with H_2 at 300 °C for 2 h and the gas hourly space velocity

(GHSV) is 1200 mL·($g_{cat.}^{-1}$ h^{-1}). The system is pressurized to 0.5 MPa with syngas. The molar ratio of syngas used is $H_2/CO/N_2 = 64/32/4$, and N_2 is used as an internal standard.

Products are analyzed online using a gas chromatograph equipped with TCD and FID detectors. The mass balance, carbon balance and nitrogen balance are kept them between 96% and 102%. The conversion of CO and the product selectivity (based on carbon number) are calculated as follows

CO conversion

$$X(CO)\% = \frac{CO(in) - CO(out)}{CO(in)}$$

The selectivity to product i is defined as

$$selectity = \frac{n_i M_i}{M_{CO,in} - M_{CO,out}}$$

where n_i is the number of carbon and M_i is the molar amount of product i detected, $M_{CO,in}$ and $M_{CO,out}$ represent the molar amount of CO at the inlet and outlet.

3. Results and discussion

3.1. Characterization of Cu_2O NCs with different shapes

3.1.1. SEM and TEM images

The reduction strategy of morphology retention is applied to synthesize identical Cu NCs from corresponding Cu_2O NCs [30]. Fig. 1 shows SEM images of the Cu_2O NCs. Uniform c-Cu_2O, o-$Cu_2O$and 18-Cu_2O are prepared by hydrothermal synthesis [30]. These structures are convinced by microscopic and spectroscopic characterizations (Fig. 1 a–f). The size distribution of c-Cu_2O, o-Cu_2O, and 18-Cu_2O is 1300 ± 200, 2000 ± 200, and 1500 ± 100 nm, respectively.

The initial Cu_2O NCs is transformed into the corresponding crystal plane metallic Cu by CO reduction (Fig. 1), while TEM and HRTEM images (Fig. 1 d–f and Fig. 1 d2–f2) show a well preservation of the morphologies of Cu NCs. The electron diffraction (ED) patterns (Fig. 1 d1–f1) verify that all acquired Cu NCs are single crystals and there are no twin crystals. As observed from the HRTEM images (Fig. 1 d2-f2), the dominant exposed planes of c-Cu are {1 0 0} and the major exposed planes of o-Cu are {1 1 1}. Another synthesized catalyst (18-Cu) is

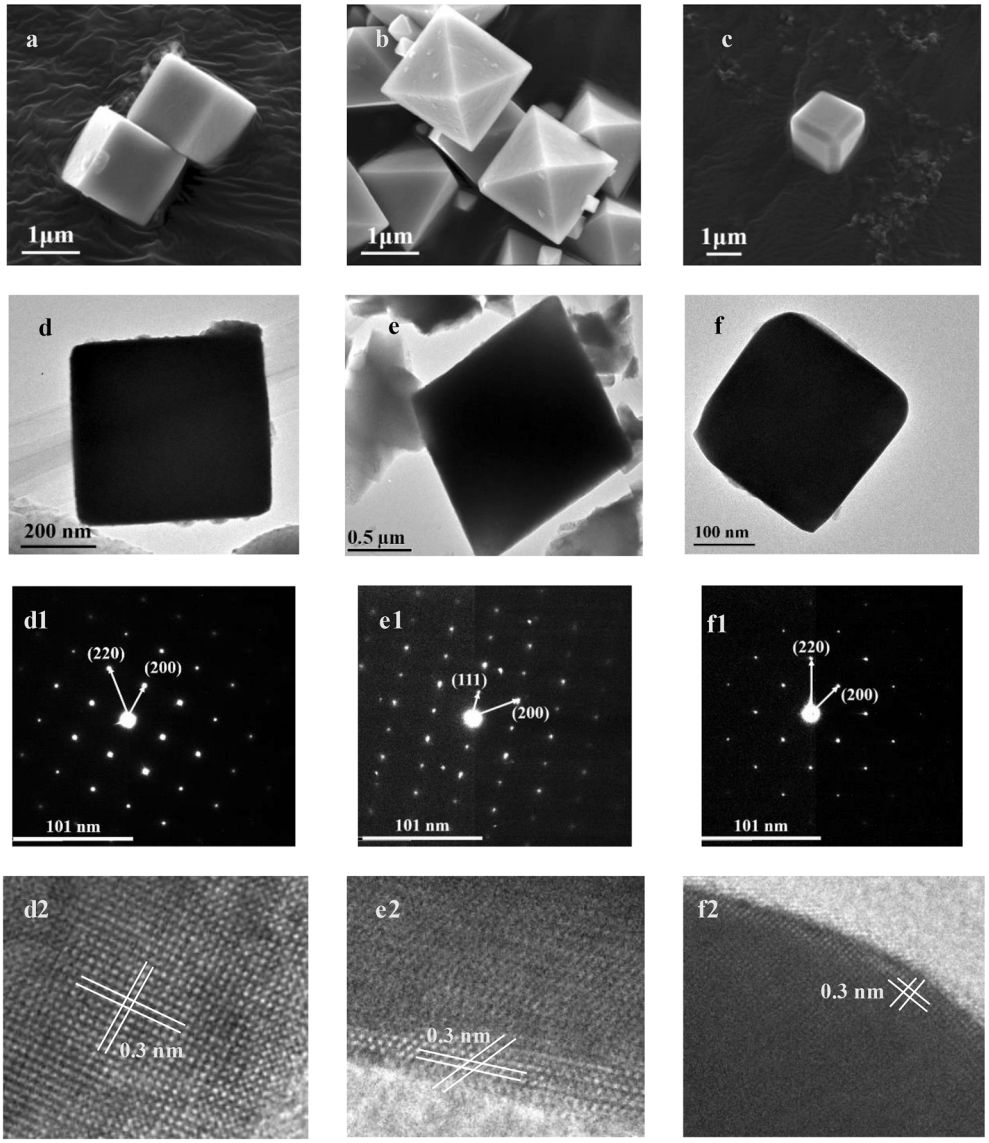

Fig. 1. Structural characterizations. The scale bars of a correspond to 1000 nm. Representative SEM images of a Cu_2O cubes (a), octahedral (b) and 18-faect (c). Representative TEM and HRTEM images of (d) c-Cu, (e) o-Cu and (f) 18-Cu. The HRTEM images of e show the ED patterns of corresponding Cu nanocrystals. The lattice fringes of 0.3 nm, respectively, correspond to the spacing of {1 0 0}, {1 1 1} and {1 0 0}&{1 1 0} crystal planes.

enclosed by 6 {1 0 0} planes and 12 {1 1 0} planes. Thus, uniform c-Cu_2O NCs, o- Cu_2O NCs and 18- Cu_2O NCs are reduced to c-Cu NCs, o-Cu NCs and 18-Cu NCs with correspondingly unchanged crystal planes, respectively.

The corresponding EDS mapping images of the Rh/P25 samples can be seen in Fig. 2. Moreover, STEM-EDS mapping characterization further confirmed the uniform distributions of Rh, Ti and O. The Rh NCs can be clearly noticed and precipitated on the surface of P25. In the HRTEM image (Fig. 2 b), the lattice fringes of 0.34 nm are attributed to the transition metal Rh, as is observed clearly in Rh/P25 catalyst. The close contact between Rh and P25 should have good conductivity to achieve a strong synergistic interaction effect. The characterization results suggest that the transition metal distribution particles on the surface of Rh/P25 catalysts are highly dispersed and similar.

3.1.2. XRD and N_2 adsorption

XRD patterns of the Cu_2O NCs with different crystal planes and Rh/P25 samples are shown in Fig. 3. As shown in Fig. 3a, clear diffraction lines can be observed in all patterns, indicating that the crystallinity of the samples is well. The three Cu_2O NCs have similar XRD patterns (Fig. 3a). No other crystalline impurities or intermediates such as Cu or CuO are discovered and it shows that the Cu_2O NCs crystals are of high purity. The XRD patterns show three different crystal planes of Cu_2O NCs expected the same (1 1 0), (1 1 1), (2 0 0), (2 2 0), (3 1 1), and (2 2 2) reflection peaks and acknowledge that these Cu_2O NCs have a cubic crystal structure.

The XRD patterns of Rh/P25 catalyst and P25 support can be seen in Fig. 3b. For the Rh/P25 catalyst, only the representative diffraction peaks of TiO_2 are observed, which means that the transition metal Rh are highly dispersed on the support P25 owing to small particles or the low contents.

The specific surface areas of the three types of Cu_2O NCs and Rh/P25 catalyst are investigated. The specific surface area, pore volume, and pore diameter of Cu_2O cubes, octahedron, and 18-facet and Rh/P25 catalyst can be seen in Table 1. The specific surface area of the three types of Cu_2O is 1.54, 1.77 and 1.07 $m^2 \cdot g^{-1}$, respectively, which are in the same scope. Therefore, the effect of BET on the reaction property of the Cu NCs catalyst can be ruled out. In addition, the BET surface area of Rh/P25 is 56.8 $m^2 \cdot g^{-1}$.

3.1.3. H_2-TPR

H_2-TPR profiles of the Rh/P25 and Cu_2O NCs are shown in Fig. 4 and reduction temperatures are listed in Table 1. Obviously, in the temperature range of 200–350 °C, all the Cu_2O NCs samples have only one reduction peak, which should be attributed to the reduction of Cu^+ into Cu^0 [30]. The peak positions are in the sequence c-Cu_2O > o-Cu_2O > 18-Cu_2O. It has been found that Cu_2O NCs show different reduction behaviors.

Compared with the H_2-TPR profiles of pure Cu_2O NCs, the reduction peaks of Rh/P25 | Cu_2O NCs catalyst shifts to lower temperatures can be observed, indicating that the reduction of Cu^+ becomes easier on the tandem catalyst Rh/P25 | Cu_2O NCs, which may be relationship with the increased lattice oxygen mobility in Cu_2O NCs, and may be related to the existence of better H_2 dissociation sites in Rh/P25 | Cu_2O NCs catalyst that promotes formation of adsorbed hydrogen atoms. Moreover, it is evident that the three Rh/P25 | Cu_2O composite samples display different reduction behaviors. Furthermore, the three Cu_2O NCs samples demonstrate a reduction peak at about 302, 297 and 278 °C, respectively. The reduction peak positions of Rh/P25 | c-Cu_2O, Rh/P25 | o-Cu_2O and Rh/P25 | 18-Cu_2O catalyst are 263, 270 and 242 °C, respectively. This indicates that the reduction behavior in Cu_2O NCs is different in these samples. The H_2-TPR profiles of these samples imply the existence of strong superposition effect between Rh/P25 and Cu_2O NCs in all the Rh/P25 | Cu_2O composites and that the superposition effect is different in the three samples.

The similar phenomenon mentioned above also appears in the H_2-

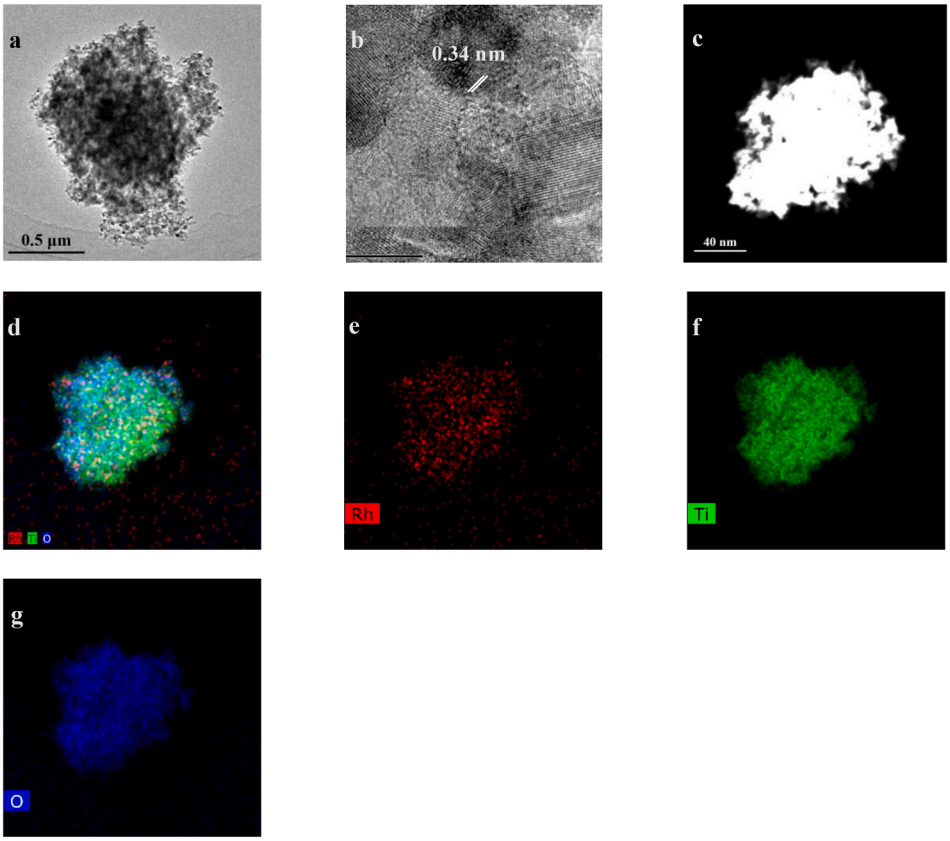

Fig. 2. HAADF-STEM overview image, HAADF-STEM image with corresponding STEM-EDX maps of Rh, Ti, O and superposition of Rh Ti and O.

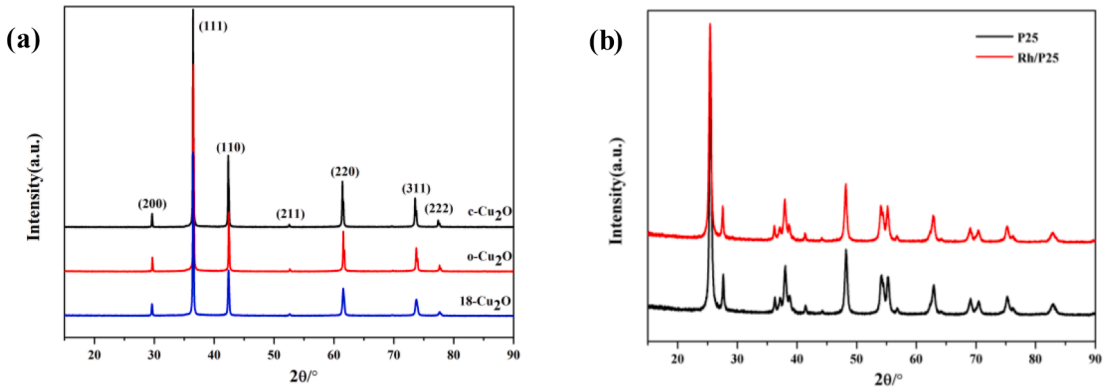

Fig. 3. (a) XRD patterns of morphologically Cu_2O microcrystals, (b) XRD patterns of P25 and Rh/P25 catalysts.

Table 1
Textural properties and H_2 chemisorption of Cu_2O NCs.

Catalysts	Surface area (BET) ($m^2 \cdot g^{-1}$)	Pore volume (cm^3/g)	Pore diameter (Å)	Reduction temperatures (°C)
c-Cu_2O	1.54	0.005	193.0	302
o-Cu_2O	1.77	0.008	190.5	297
18-Cu_2O	1.07	0.005	192.1	278
Rh/P25	56.8	0.175	122.8	161

[a]by H_2-chemisorption method.

TPR profiles of Rh/P25 + Cu_2O catalyst. The reduction peaks of Rh/P25 + Cu_2O catalyst shifted to lower temperatures and the three physical particle mixing samples show different reduction behaviors. For Rh/P25 + c-Cu_2O catalyst, the reduction peak shifts from 302 to 226 °C. Besides, For Rh/P25 + o-Cu_2O catalyst, the reduction peak shifts from 297 to 229 °C. For Rh/P25 + 18-Cu_2O catalyst, the peak position shifts from 278 to 235 °C. All the H_2-TPR profiles show the existence of strong superposition effect between Rh/P25 and Cu_2O NCs in the Rh/P25 | Cu_2O and Rh/P25 + Cu_2O composites.

3.1.4. *Diffuse reflectance Fourier transform infrared (DRFTIR) spectra*

DRFTIR spectra of the H_2 in-situ reduction of Rh/P25 and Cu NCs catalysts after CO adsorption for 30 min at 30 °C is shown in Fig. 5, where no obvious impurities are detected, illustrating the formation of pure Cu_2O. The vibration bands of 2117 cm^{-1} is noticed on c-Cu_2O {1 0 0}, o-Cu_2O{1 1 1} and 18-Cu_2O{1 0 0}&{1 1 0} facets and is assigned as CO adsorbed at the Cu^+ sites, which is consistent with previous reports [31,32]. Considering that no Cu^{2+} existed in the reduced samples, the bands centered at around 2170 cm^{-1} is attributed to gas phase CO adsorption peak, as shown in Fig. 5 a, b and c. As shown in Fig. 5b, the vibration bands of 2109 cm^{-1} was observed on c-Cu_2O and assigned to CO-adsorbed at the Cu (I) sites. It is located at 2092 cm^{-1} on o-Cu, 2018 cm^{-1} on c-Cu and 18-Cu that respectively correspond well to that of CO adsorbed on Cu (1 1 1), (1 0 0), and (1 1 0) single-crystal surfaces [33,34]. In addition, Cu^0 promotes H_2 dissociation and Cu^+ can stabilize acetyl and methyl, as has been reported [35]. Therefore, the CO adsorbed on Cu^+ will damage the balance between Cu^0 and Cu^+, resulting in a decrease in catalytic activity [36].

When the Rh/P25 and Cu catalyst is physically mixed, the intensity of the CO adsorption peak ($Cu^+(CO)$) increases. It implies that the physical mixing of the catalyst can increase the adsorption of carbon monoxide. Infrared spectra of sequential irreversible CO adsorption on Rh/P25 at 30 °C are presented in Fig. 5. In addition, the bimodal characteristics of CO between 2170 and 1800 cm^{-1}, the characteristic bands of three adsorption states of CO can be determined: $Rh^+(CO)_2$, linearly adsorbed CO and bridge-adsorbed CO on Rh^0. Interestingly, at 30 °C, there is clear evidence of cationic $Rh^{\delta+}$ even after reduction at 300 °C. In the DRIFTS spectra of Rh/P25 catalyst, the strong bands at 2092 and 2028 cm^{-1} are assigned to the symmetric and asymmetric vibrations of gem-dicarbonyl species $Rh^+(CO)_2$ [CO(gdc)] on the Rh^+ sites which may be formed on highly dispersed Rh [37,38]. Further, for linearly absorbed CO on Rh^0, the broad band around 1803 cm^{-1} indicates the presence of bridge CO [CO(b)] on Rh^0 at 30 °C [39]. The characteristic broad feature of this band has been ascribed to CO adsorption on different Rh crystalline faces, such as Rh(1 0 0) and Rh (1 1 1). At 30 °C, the most prominent feature that does not appear is the vibrational frequency at 2059–2070 cm^{-1}, which is attributed to linearly bonded CO [CO(l)] adsorbed on reduced Rh metal (Fig. 5). However, for the physical mixed catalysts, the adsorption strength of CO

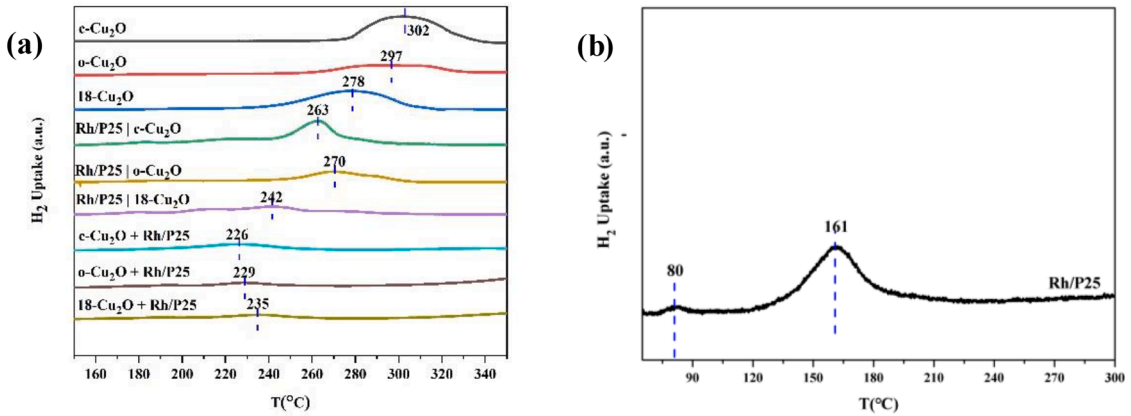

Fig. 4. (a) H_2-TPR profiles of Cu_2O, Rh/P25 | Cu_2O and Rh/P25 + Cu_2O composites; (b) H_2-TPR profiles of various Rh/P25 composites.

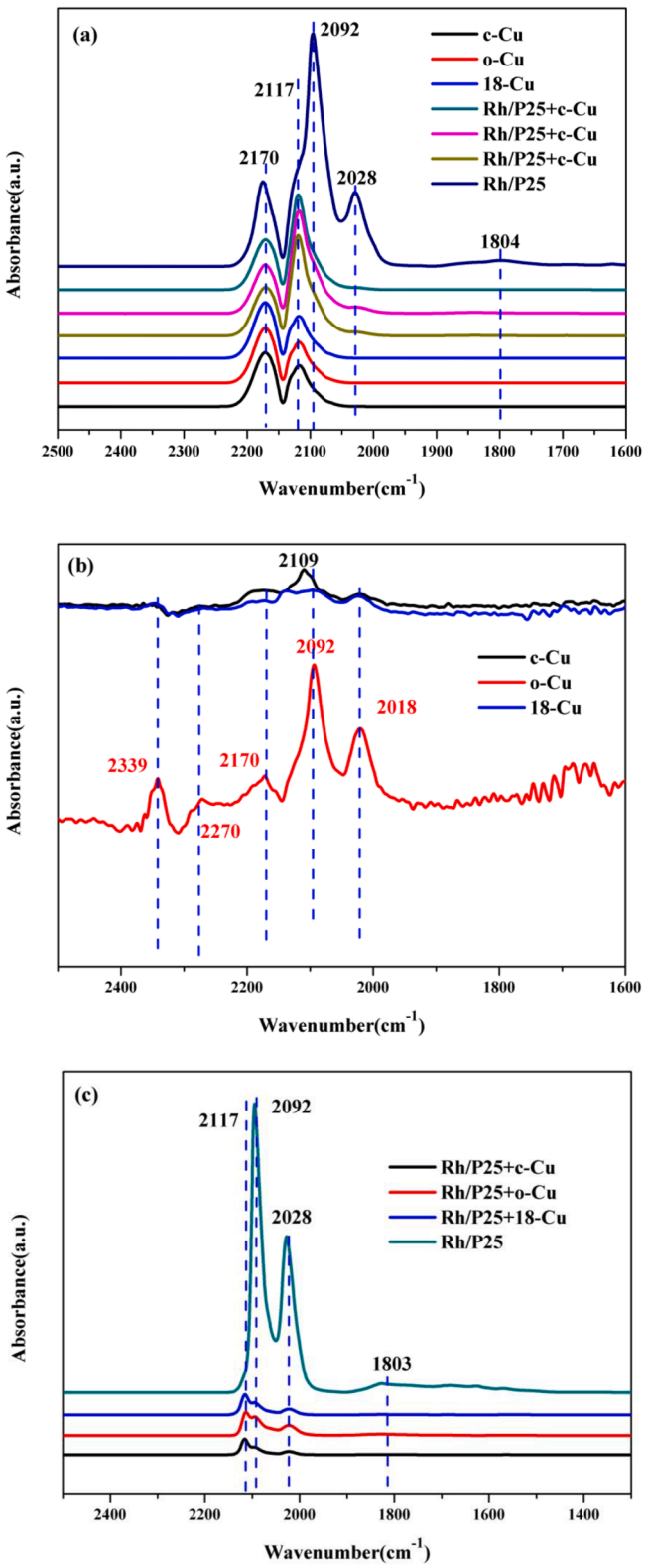

Fig. 5. In situ DRIFTS spectra of CO adsorption at 30 °C of catalysts: (a) No Ar purging, (b) Ar purging for 30 min, (c) Ar purging for 30 min.

(gdc) decreased and the CO(b) adsorption peak disappeared (Fig. 5c).

As observed, the CO band at 2092 and 2028 cm^{-1} on Rh/P25 + Cu_2O NCs catalyst decreased rapidly at first. At the same time, the intensity of CO decreased, along with the band disappear at around 1803 cm^{-1}. By combining the catalytic properties of the Rh/P25 + Cu_2O NCs catalyst, it can be deduced that the catalytic performances of the Rh/P25 + Cu_2O NCs catalyst are related to the desorption or transformation behavior of the $Rh^{+}(CO)_2$ bands in the reaction.

3.1.5. XPS spectra

The XPS spectra of the three types of Cu_2O NCs are demonstrated in Fig. 6. No Cu^{2+} feature is observed in the Cu 2p XPS spectra. The binding energies (BEs) of Cu $2p_{3/2}$ and Cu $2p_{1/2}$ in Cu 2p spectra is nearly almost the same for the three fresh Cu_2O NCs and which are located at 933.2 and 952.3 eV, respectively. In the O 1s XPS spectra, three components appear with the O 1s BEs at 529.5, 530.3 and 531.8 eV that can be assigned to oxygen adsorption atoms separately, Cu suboxide, and OH groups or oxygenates species; in the C 1s XPS spectra, adventitious carbon, carbonate and carboxylate species with the C 1s BEs at 284.8, 288.9 and 287.7 eV, respectively, are visible for all Cu NCs. XRD patterns and Cu 2p XPS spectra exhibited the same features for as-synthesized Cu_2O NCs.

3.1.6. CO-TPD

The TPD-MS profiles of catalyst for CO desorption, and relative information are shown in Figs. 7–9. We can find that the one peak of CO desorption weakly existed on Cu NCs catalysts, corresponding to different temperatures: high temperature site (at about 558 °C), but no peak of CO desorption existed on 18-Cu NCs catalysts. Moreover, low temperature sites (at about 130 °C) could be observed on Rh/P5 + Cu NCs catalysts. According to the research reported previously [40,41], it is suggested that low temperature site may correspond to the CO(l) species, medium temperature site may be due to CO(gdc) species and high temperature site may be assigned to the CO(b) species.

It can be seen that the Rh/P25 | Cu NCs tandem catalysts greatly weakened the desorption peak intensity of CO(l), while comparatively strengthened the peak intensity of CO(gdc) on the Rh/P25 | o-Cu NCs and Rh/P25 | 18-Cu NCs tandem catalysts. The results indicated that the Rh/P25 | o-Cu NCs and Rh/P25 | 18-Cu NCs tandem catalysts could effectively strengthen the CO adsorption and coordinate the relative proportion of CO(l), CO(gdc) and CO(b) species, which may be crucial for improved catalytic activity and ethanol selectivity.

In summary, combining all the above characterization results shows uniform c-Cu_2O{1 0 0}, o-Cu_2O{1 1 0} and 18-Cu_2O{1 0 0}& {1 1 0} facets have been successfully synthesized, and c-Cu{1 0 0}, o-Cu{1 1 1}, and 18-Cu{1 0 0}&{1 1 0} facets are synthesized by a morphology retention reduction of corresponding c-Cu_2O, o-Cu_2O, and 18-Cu_2O NCs.

3.2. Catalytic performance of different Cu NCs

The catalytic performance and product distribution of the three types of Cu NCs catalyst are studied in Fig. 10 and Table 2. These Cu NCs catalysts have similar surface areas which cannot be explained as the reason for the significant change in catalytic performance. Thus, the significant difference in catalytic activity of c-Cu, o-Cu and 18-Cu can be attributed to the different crystal plane of the Cu NCs catalysts. Under our reaction conditions, the c-Cu, o-Cu and 18-Cu NCs exhibited a CO conversion of 4.6%, 4.1%, 9.1% and a CH_4 selectivity of 23.3%, 23.6%, 20.9%, respectively. The selectivity of C_2H_5OH and CH_3OH over these catalysts are 0.9%, 0.3%, 0.5% and 14.8%, 15.4%, 11.2%, respectively. The order of CH_4 and methanol selectivity is established as {1 0 0}& {1 1 0} < {1 0 0} < {1 1 1}, which are a highly undesirable by-product. The three catalysts showed higher selectivity to CO_2. For c-Cu, o-Cu and 18-Cu, indicating that the 18-Cu with exposed {1 0 0}&{1 1 0}facets exhibits higher activity in comparison to the other Cu NCs catalysts at 240 °C. The evaluated CO hydrogenation results demonstrate that different Cu NCs exhibit different facet-dependent catalytic activity for ethanol synthesis from carbon monoxide hydrogenation. However, these three Cu NCs have the low activity for ethanol synthesis from carbon monoxide hydrogenation. Therefore, so as to improve the CO conversion and C_2H_5OH selectivity, we chose the combination of Rh/

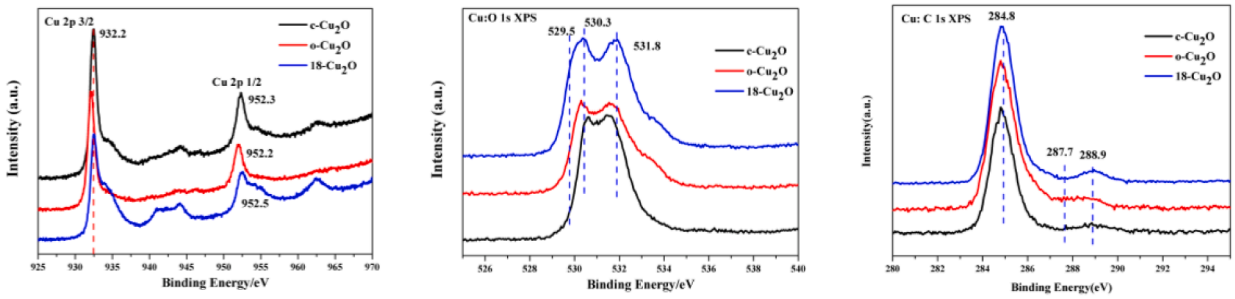

a. Cu 2p XPS spectra b. O 1s XPS spectra c. C 1s XPS spectra

Fig. 6. XPS spectra of the three types of Cu_2O NCs.

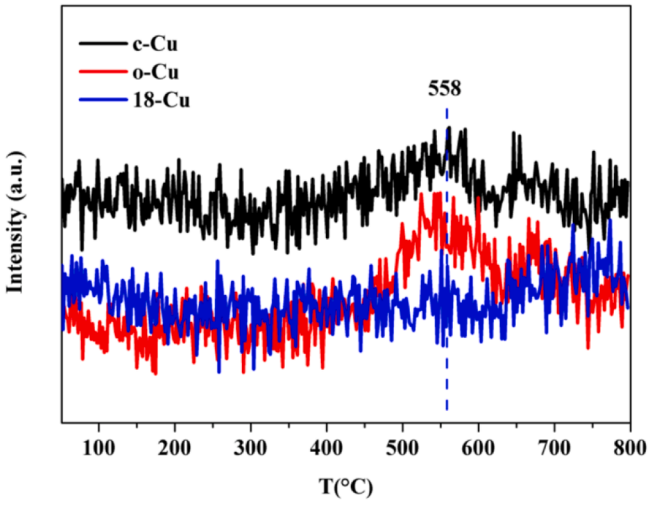

Fig. 7. TPD-MS profiles of Cu NCs catalysts for CO desorption.

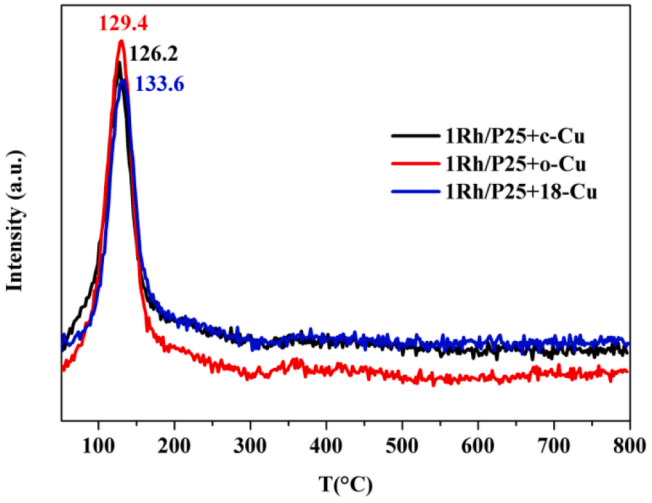

Fig. 8. TPD-MS profiles of Rh/P25 + Cu NCs catalysts for CO desorption.

P25 catalyst and different Cu NCs for further studies.

3.3. Catalytic performance of Rh/P25 and Cu_2O NCs physical particle mixing catalyst

Here, the ethanol synthesis process as evaluated with syngas over

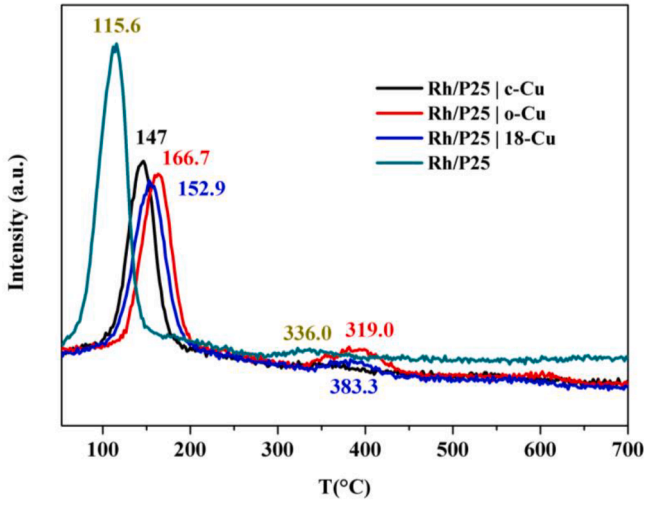

Fig. 9. TPD-MS profiles of Rh/P25 | Cu NCs catalysts and Rh/P25 catalyst for CO desorption.

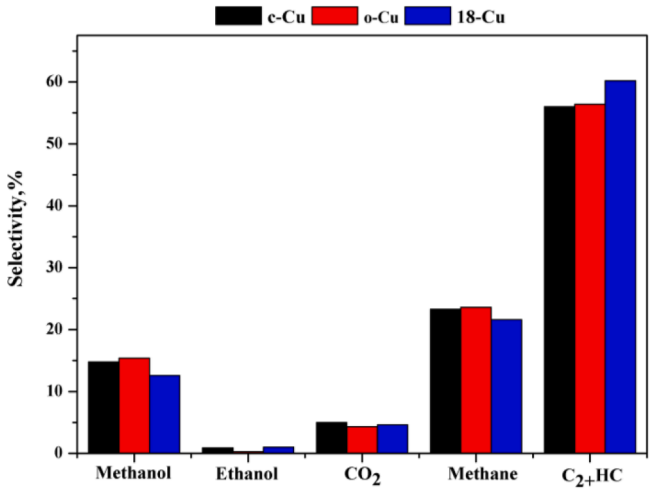

Fig. 10. Products selectivity (% carbon efficiency) for CO hydrogenation over c-Cu, o-Cu and 18-Cu catalysts (reaction conditions: weight $_{Cu}$ = 0.5 g, T = 240 ℃, P = 0.5 MPa, GHSV = 1200 mL·h^{-1}·g$^{-1}_{cat}$, H_2/CO = 2/1).

Rh/P25catalysts. The catalytic performance of pure Rh/P25 catalyst for the synthesis of ethanol from syngas at different temperatures is studied in Table S1 and Fig. S1. Since P25 support is inactive for syngas conversion under reaction conditions, therefore, the product formation

Table 2
Products selectivity (% carbon efficiency) for CO hydrogenation over different Cu NCs catalyst.

Catalysts	Conversion (%)	Selectivity (%)				
		CH_3OH	EtOH	CO_2	CH_4	$C_{2+}HC$[a]
c-Cu	4.6	14.8	0.9	5.0	23.3	56.0
o-Cu	4.1	15.4	0.3	4.3	23.6	56.4
18-Cu	9.1	12.6	1.0	4.6	21.6	60.2

[a] Hydrocarbons with two or more carbons.

observed in this study is only owing to the interaction of the transition metal with the support. With the temperature increases, the selectivity of ethanol rises from 10.7% to 13.4% and CO conversion also increased. This is illustrated in Table S1, the production of other hydrocarbons increased after 260 °C, indicating that the catalyst ethanol selectivity is reduced owing to the hydrocarbon chain growth process on the Rh/P25 catalyst. Hence, the experimental results show that the selectivity of CH_4 increases, while the selectivity of ethanol first increases and then decreases with increasing temperature.

For the purpose of studying the effect of Rh/P25 and Cu NCs with different crystal planes for ethanol direct synthesis from syngas, the catalytic performances of physical particle mixing catalysts are measured. As shown in Fig. 11, Fig. 12 and Table 3, the product selectivity and the CO conversion is given. Under the physical particle mixing mode, it is found that the conversion of CO first increase and a higher selectivity of ethanol at 240 °C is obtained.

For the combination of pure Rh/P25 catalyst and Cu NCs with different facet, the CO conversion is 27.5%, 21.9%, 39.0% and the selectivity of ethanol is 15.7%, 14.7%, 15.1% over Rh/P25 + c-Cu, Rh/P25 + o-Cu and Rh/P25 + 18-Cu catalysts, respectively. A higher CO conversion of 39.0% is achieved in the reactor, where Rh/P25 + 18-Cu catalyst has the best performance for ethanol synthesis from carbon monoxide hydrogenation. And it seems that the physically mixed of Rh/P25 + 18-Cu catalyst seems to be more active than the pure Rh/P25 catalyst for the ethanol synthesis from syngas under the same reaction condition. The single Rh/P25 catalyst presented a lower CO conversion of 27.9%, as shown in Table 3. Evaluation results display that the synergy of the two catalysts may increase the selectivity of ethanol. Compared with the pure Rh/P25 catalyst, the ethanol selectivity of the Rh/P25 + 18-Cu catalyst is increased from 12.4% to 15.1%, while CH_3OH selectivity decreased from 30.1% to 24.9%, which indicated that the Rh/P25 + 18-Cu catalyst is more conducive to ethanol synthesis. In addition, other by-products, such as methyl acetate (MA), dmethyl ether (DME), CO_2, CH_4 and $C_{2+}HC$, are also present in the final products.

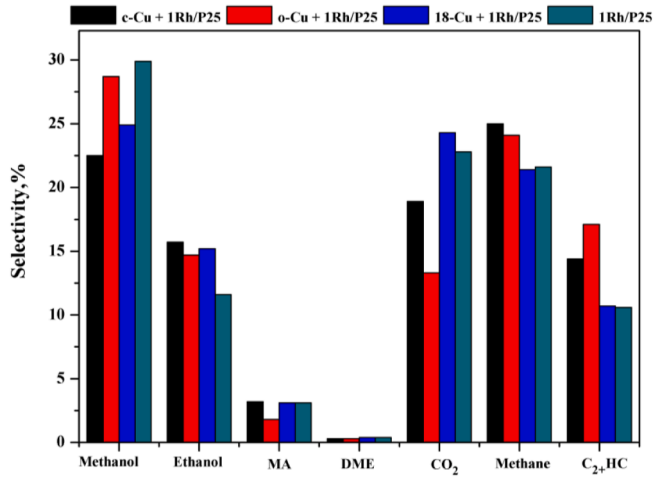

Fig. 11. Products selectivity (% carbon efficiency) for CO hydrogenation over Rh/P25, Rh/P25 + c-Cu, Rh/P25 + o-Cu and Rh/P25 + 18-Cu catalysts (reaction conditions: weight $_{Rh/P25}$ = 0.5 g, weight $_{Rh/P25\ +\ Cu}$ = 1.0 g, T = 240 ℃, P = 0.5 MPa, GHSV = 1200 mL·h^{-1}·g$^{-1}_{cat}$, H_2/CO = 2/1).

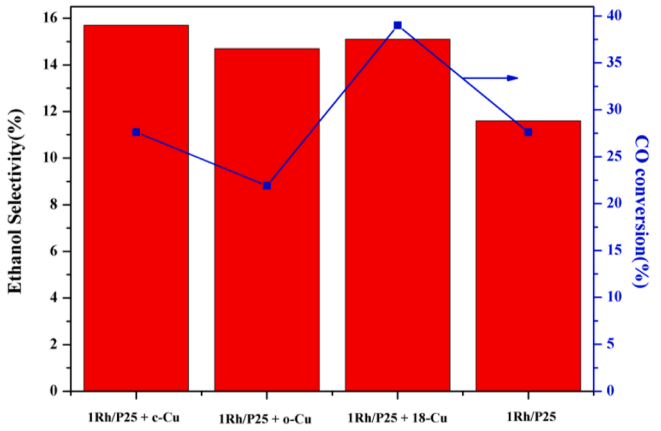

Fig. 12. Products ethanol selectivity (% carbon efficiency) for CO hydrogenation and CO conversion rate over Rh/P25, Rh/P25 + c-Cu, Rh/P25 + o-Cu and Rh/P25 + 18-Cu catalysts (reaction conditions: weight $_{Rh/P25}$ = 0.5 g, weight $_{Rh/P25\ +\ Cu}$ = 1.0 g, T = 240 ℃, P = 0.5 MPa, GHSV = 1200 mL·h^{-1}·g$^{-1}_{cat}$, H_2/CO = 2/1).

The MA selectivity is only 3.3%, 1.8%, 3.2% in final products, slightly lower than single Rh/P25 catalyst, indicating that the formed methyl acetate from Rh/P25 and Cu NCs physical particle mixing catalyst is suppressed. It is worth noting that CH_3OH as the main by-product with the selectivity of 22.5%, 28.7% and 24.9%, respectively, over Rh/P25 + c-Cu, Rh/P25 + o-Cu and Rh/P25 + 18-Cu catalysts, is prepared by CO hydrogenation, but here the selectivity of CH_3OH is lower than pure Rh/P25 catalysts. Therefore, for the combination of pure Rh/P25 catalyst, the physical mixing of Rh/P25 and Cu NCs can obviously inhibit the formation of methanol.

3.4. Catalytic performance of Rh/P25 and Cu_2O NCs tandem catalyst

In order to study the impact of different crystal-plane Cu NCs on conversion of syngas to ethanol, the catalytic performances of Rh/P25 and Cu_2O NCs tandem catalysts are measured in Fig. 13, Fig. 14 and Table 4. Here, we discovered the Rh/P25 and Cu_2O NCs tandem catalysts for ethanol synthesis (Scheme 1(b)). In tandem mode, the conversion of CO first increase, and a higher selectivity of the target product ethanol at 240 °C is obtained, which means that the formation of by-products is suppressed.

For the combination of pure Rh/P25 catalyst and Cu catalyst with different facet, the CO conversion is 34.9%, 28.2%, 43.4% and the selectivity of ethanol is 13.9%, 14.0%, 18.7% over Rh/P25 | c-Cu, Rh/P25 | o-Cu and Rh/P25 | 18-Cu catalysts, respectively. A higher CO conversion of 43.4% is achieved in the tandem catalyst, where Rh/P25 | 18-Cu catalyst has the best performance for ethanol synthesis from carbon monoxide hydrogenation. The results show that the Rh/P25 | 18-Cu catalyst is more active than the pure Rh/P25 catalyst for the ethanol synthesis from syngas under the same reaction condition. These results may be due to the superimposition of two consecutive reactions that promote the increase in ethanol selectivity. Compared with the single Rh/P25 catalyst, the ethanol selectivity of the tandem catalyst Rh/P25 | 18-Cu is increased from 12.4% to 18.7% and the selectivity of CH_3OH from 30.1% to 26.0%, which indicated that the Rh/P25 | 18-Cu catalyst is more conducive to ethanol synthesis from syngas under the same reaction conditions. Moreover, other by-products, such as DME, MA, CO_2, CH_4 and $C_{2+}HC$, are also present in the final products.

The MA selectivity are only 3.0%, 2.0%, 3.7% in final products, respectively, slightly lower than that of single Rh/P25 catalyst, indicating that the formed methyl acetate from Rh/P25 catalyst may have reacted on the Cu NCs catalyst. It is worth noting that CH_3OH as the

Table 3
Products selectivity (% carbon efficiency) for CO hydrogenation over Cu NCs catalyst.[a]

Catalysts	Conversion (%)	Selectivity (%)						
		CH_3OH	EtOH	MA	DME	CO_2	CH_4	$C_{2+}HC$
Rh/P25 + c-Cu	27.5	22.5	15.7	3.3	0.4	18.9	25.0	14.2
Rh/P25 + o-Cu	21.9	28.7	14.7	1.8	0.3	13.3	24.0	17.1
Rh/P25 + 18-Cu	39.0	24.9	15.1	3.2	0.4	24.3	21.4	10.7
Rh/P25	27.9	30.1	12.4	4.2	0.3	22.1	20.8	10.1

[a] Reaction conditions: weight $_{Rh/P25+Cu}$ = 1 g, T = 240 ℃, P = 0.5 MPa, GHSV = 1200 mL·h^{-1}·g$^{-1}_{cat}$, H_2/CO = 2/1.

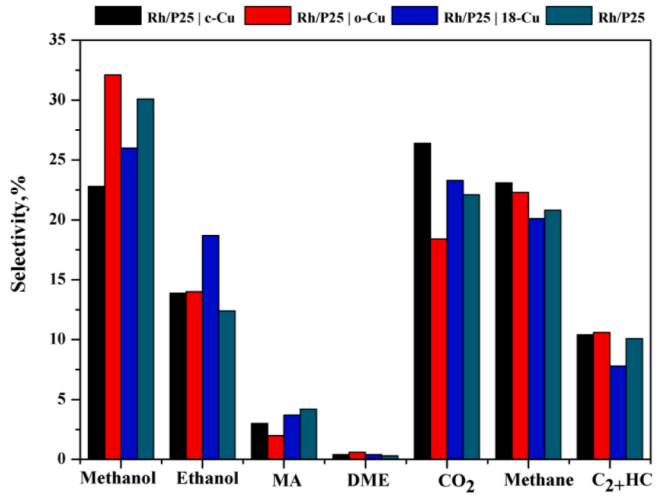

Fig. 13. Products selectivity (% carbon efficiency) for CO hydrogenation over Rh/P25, c-Cu, o-Cu, 18-Cu, Rh/P25 | c-Cu, Rh/P25 | o-Cu and Rh/P25 | 18-Cu catalysts (reaction conditions: weight $_{Rh/P25}$ = 0.5 g, weight $_{Cu}$ = 0.5 g, weight $_{Rh/P25\ |\ Cu}$ = 1.0 g, T = 240 °C, P = 0.5 MPa, GHSV = 1200 mL·h^{-1}·g$^{-1}_{cat}$, H_2/CO = 2/1).

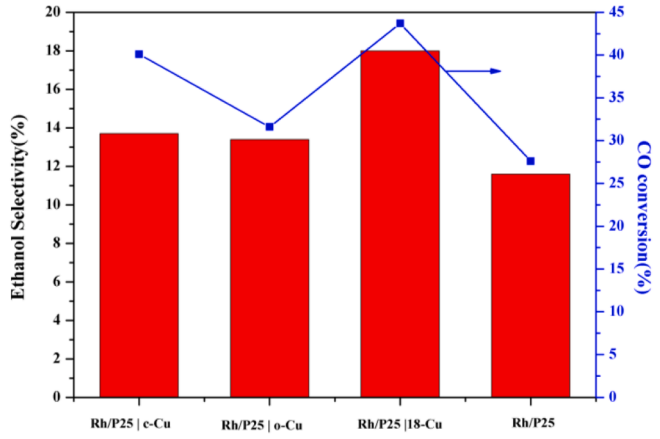

Fig. 14. Products ethanol selectivity (% carbon efficiency) for CO hydrogenation and CO conversion rate over Rh/P25, Rh/P25 | c-Cu, Rh/P25 | o-Cu and Rh/P25 | 18-Cu catalysts (reaction conditions: weight $_{Rh/P25}$ = 0.5 g, weight $_{Rh/P25\ |\ Cu}$ = 1.0 g, T = 240 ℃, P = 0.5 MPa, flow rate = 1200 mL·h^{-1}·g$^{-1}_{cat}$, H_2/CO = 2/1).

main by-product with the selectivity of 22.8% and 26.0%, respectively, over Rh/P25 | c-Cu and Rh/P25 | 18-Cu catalysts, is generated by CO hydrogenation, but here the selectivity of CH_3OH is lower than pure Rh/P25 catalysts. The selectivity of methanol over Rh/P25 | o-Cu is higher than pure Rh/P25 catalysts. The experimental results show that the Cu NCs on the lower layers exhibits different crystal plane effects over combined Rh/P25 and Cu NCs Catalysts.

In general, according to results on the Cu NCs catalyst, we can conclude that the Rh/P25 and Cu NCs tandem catalyst is more favorable than Rh/P25 + Cu_2O physical particle mixing catalyst and single Cu NCs catalyst for ethanol synthesis from carbon monoxide hydrogenation. Since the trend of the ethanol selectivity and catalytic activity, Cu-based catalysts with different crystal faces has been established as Cu{1 1 1} < Cu{1 0 0} < Cu{1 0 0}&{1 1 0}. Furthermore, it is widely accepted that the catalytic performance of the ethanol synthesis from syngas can be enhanced by combined Rh-based and Cu-based catalysts.

3.5. Probe molecule experiments

3.5.1. Effect of methanol as probe molecule

The Rh/P25 and Rh/P25 | 18-Cu model catalyst was first evaluated without addition of any probe molecule agents. The CO conversion and ethanol selectivity were 27.7%, 43.4% and 12.4%, 18.7% (Table 4), respectively, in accordance with our reported catalysts. In order to study the effect of co-feeding methanol (0.01 mL/min) and syngas on the performance of ethanol synthesis on 18-Cu NCs catalyst, a probe experiment with methanol as the probe molecule was conducted. Upon the addition of methanol, 2.5% of CO conversion, 9.7% of methanol selectivity and no ethanol were obtained (Table 5), similar to the results of the experiment without probe molecules, suggesting that methanol was not reactive in this catalytic system.

In our experiment, the added methanol was not excluded from the calculation of total alcohol distribution. The total alcohol distribution of the collected products with methanol addition are shown in Table 5. It could be seen that the selectivity of total alcohols and methanol is reduced when methanol was added. In addition, the co-feeding of methanol and syngas did not increase the selectivity of ethanol on the 18-Cu NCs catalyst, but inhibited the formation of methanol.

3.5.2. Effect of methyl acetate (MA) as probe molecule

Upon the addition of co-feeding of MA (0.01 mL/min) and syngas as the probe molecule on 18-Cu NCs, the CO conversion and alcohol selectivity increased slightly compared with pure syngas addition. However, CO_2 selectivity decreased and a small amount of ethanol (5.1%, Table 5) was formed. In addition, when pure MA was added, no ethanol was detected in our system. These results suggested that the added MA participated in the reaction leading to new reaction pathways to form ethanol. This indicated that the added MA participated in the reaction to form the ethanol.

Note that the mole fraction of MA produced on the Rh/P25 catalyst does not match the mole fraction of methyl acetate added from the outside, the mole fraction of the product MA in the 18-Cu catalyst is not considered and only the formation of alcohol is considered. The effect of MA addition on alcohol distribution was also investigated. As shown in Table 5, the methanol and ethanol distribution were almost changed with the addition of MA, indicating that the effect of MA addition on alcohol distribution can be not ignored.

3.5.3. Effect of dimethyl ether (DME) as probe molecule

DME as the model probe molecule was also added. When 1% DME was added, CO conversion decreased sharply from 9.1% to 1.5% compared with pure syngas (Table 5). In addition, ethanol selectivity

Table 4
Products selectivity (% carbon efficiency) for CO hydrogenation over Rh/P25 and Cu tandem catalyst.[a]

Catalysts	Conversion (%)	Selectivity (%)						
		CH_3OH	EtOH	MA	DME	CO_2	CH_4	$C_{2+}HC$
Rh/P25 | c-Cu	34.9	22.8	13.9	3.0	0.4	26.4	23.1	10.4
Rh/P25 | o-Cu	28.2	32.1	14.0	2.0	0.6	18.4	22.3	10.6
Rh/P25 | 18-Cu	43.4	26.0	18.7	3.7	0.4	23.3	20.1	7.8
Rh/P25	27.9	30.1	12.4	4.2	0.3	22.1	20.8	10.1

[a] Reaction conditions: weight $_{Rh/P25\ |\ Cu}$ = 1 g, T = 240 ℃, P = 0.5 MPa, GHSV = 1200 mL·h^{-1}·g$^{-1}_{cat}$, H_2/CO = 2/1.

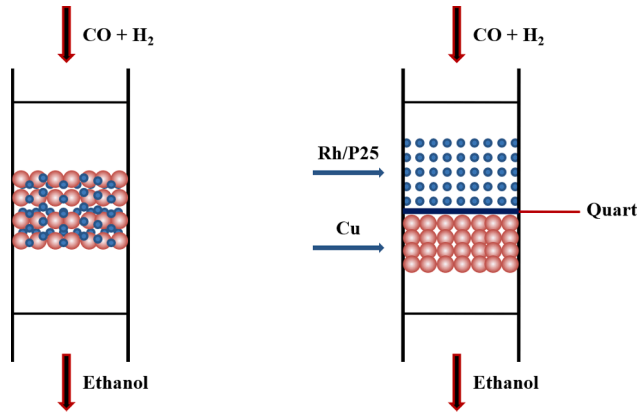

(a) Rh/P25 + Cu NCs **(b) Rh/P25 | Cu NCs**

Scheme 1. Illustration of catalyst loading in reactor: (a) the physical mixing catalyst for ethanol synthesis and (b) the dual-catalyst bed reactor for ethanol synthesis.

increased to 2.5%, which mainly resulted from the direct syngas and DME to methanol and ethanol. However, when the syngas in added DME was excluded, there is no alcohol formed on 18-Cu NCs catalyst. Some studies have demonstrated that the co-feeding of DME and syngas over dual-bed catalysts for DME carbonylation and methyl acetate hydrogenation provided ethanol [28,42,43]. Briefly, DME was firstly converted to MA intermediate through carbonylation on Rh/P25 catalyst in the first stage of the reactor, and then the formed MA was hydrogenated to EtOH on a Cu-based catalyst in the second stage of the reactor. These two reactions at different stages can be described as follows:

$$CO+CH_3OCH_3 \rightarrow CH_3COOCH_3 \quad (1)$$

$$CH_3COOCH_3+2H_2 \rightarrow CH_3CH_2OH+CH_3OH \quad (2)$$

Therefore, our molecular probe experiments prove that DME and MA may be an intermediate product that promotes ethanol selectivity on tandem catalysts.

3.6. Discussion of catalytic mechanism and reaction network

Probe molecule experiment is widely used in mechanistic investigations. With their perturbation on the reaction, probe molecules could provide insightful information on the reactive intermediates and reaction pathways. Ethanol synthesis is very complicated with many parallel and consecutive reactions. In order to explore the reaction network and catalytic mechanism during the ethanol synthesis from syngas process, probe molecule experiments over 18-Cu NCs catalyst were carried out. It showed that the MA, CH_3OH and DME alone had almost no effect on the reaction. However, the reactive agents (MA and DME) with syngas greatly affected the reaction network.

In the probe molecule experiments with MA, a small amount of ethanol was formed. This indicated that the added MA participated in the reaction to form the ethanol. Since no detectable acid was found in the products, the esters seemed unlikely to be formed by the reaction between acids and methanol. It was very likely that the added MA reacted with syngas directly to form the ethanol, indicating the existence of surface acyl species.

The statement that ethanol was further confirmed by using DME as the probe molecule. A small amount of ethanol was formed indeed when DME was added (Table 5). In the DME probe experiments, though a small amount of DME was added, only 1.5% of DME species was trapped to form ethanol while most of the species were converted to $C_{2+}HC$. Nevertheless, the production of ethanol in the case of MA and DME as probe molecules indicated the existence of intermediate species on the Rh/P25 catalyst move to 18-Cu NCs catalyst, which increases the selectivity of ethanol over 18-Cu NCs catalyst.

Based on the above discussion, the reaction network of the ethanol process was summarized over Rh/P25 | 18-Cu catalysts as described in Scheme 2. Ethanol formation needs two active sites as dual-sites, on which one active site functions for CO dissociation and chain propagation (M_1 site), while the other one functions for CO non-dissociative activation and insertion (M_2 site). In addition, the intermediate products (MA and DME) may be transferred to the 18-Cu catalyst along with the syngas, which increases the selectivity of ethanol. The new intermediate species also get involved in the reaction network and incorporate products in various reactions on the tandem catalyst.

4. Conclusions

We successfully designed a tandem catalytic system (combined Rh-based and Cu-based catalysts) which has higher target product selectivity for ethanol synthesis directly from syngas. The results show that the tandem catalysts (Rh/P25 | Cu NCs) are more favorable than single Rh/P25 catalyst and single Cu NCs catalyst for ethanol synthesis from

Table 5
Catalytic performances of over 18-Cu in syngas synthesis ethanol reaction with different probe molecules.

Catalyst	Probe molecule	Conversion (%)	Selectivity (%)				
			CH_3OH	EtOH	CO_2	CH_4	$C_{2+}HC$
18-Cu{100}&{110}	CO + H_2	9.1	12.6	1.0	4.6	21.6	60.2
	CO + H_2 + CH_3OH	2.5	9.7	–	3.2	36.0	51.1
	CH_3OH	–	–	–	–	–	–
	CO + H_2 + MA	2.1	28.1	5.1	0.4	43.6	22.8
	MA	–	–	–	–	–	
	CO + H_2 + DME (1%)	1.5	2.6	2.5	8.6	13.5	72.8
	DME (1%)	–	–	–	–	–	–

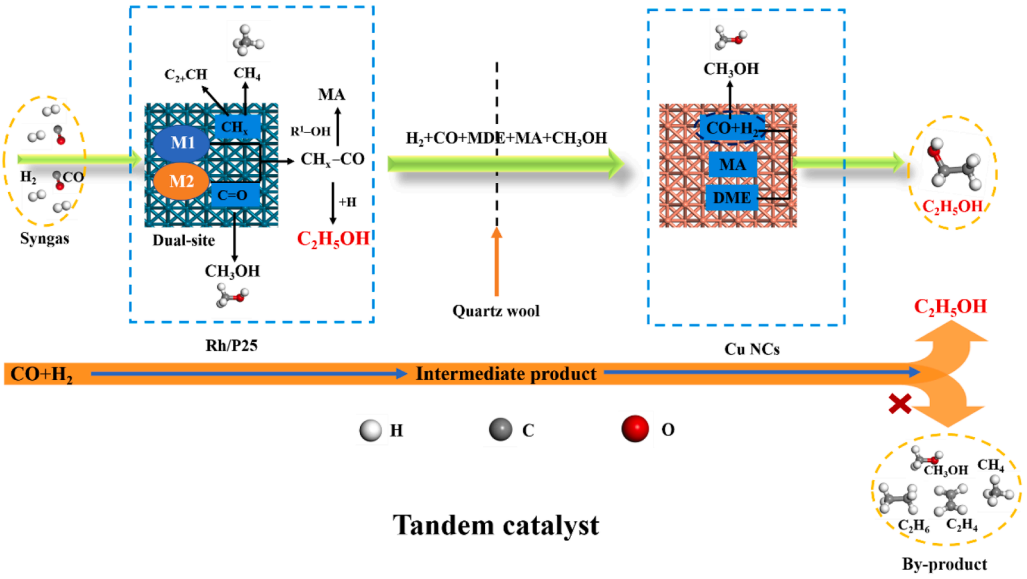

Scheme 2. Schematic depiction of the reaction network and active site over Rh/P25 | Cu NCs tandem catalyst during syngas synthesis ethanol reaction.

carbon monoxide hydrogenation. The physical blending catalysts not only can slightly improve the catalytic performance but also the ethanol selectivity. Results show that the Rh/P25 | 18-Cu{1 0 0}&{1 1 0} facet exhibit the best activity (43.4%) and ethanol selectivity (18.7%). It may be that the synergistic effect of Rh-based catalyst and Cu catalyst promotes the increase of ethanol selectivity. The crystal plane-dependent catalytic performance of the Cu NCs in the tandem reaction for the ethanol synthesis from CO hydrogenation are also explored and confirmed by the characterization of the experimental structure. The probe experiments reveal that the intermediate products (MA and DME) may be transferred to the 18-Cu catalyst along with the syngas, which increases the selectivity of ethanol. The current work provides an effective method to increase the ethanol selectivity from CO hydrogenation.

CRediT authorship contribution statement

Yang Feng: Writing – original draft, Writing – review & editing, Formal analysis. **Jungang Wang:** Writing – review & editing, Data curation. **Lixia Ling:** Writing – review & editing, Data curation. **Bo Hou:** Formal analysis. **Riguang Zhang:** Formal analysis, Funding acquisition. **Debao Li:** Conceptualization, Resources, Software, Project administration, Supervision. **Baojun Wang:** Data curation, Conceptualization, Funding acquisition, Resources, Supervision.

Declaration of Competing Interest

The authors declare that they have no known competing financial interests or personal relationships that could have appeared to influence the work reported in this paper.

Acknowledgements

This work is financially supported by the Key Program of National Natural Science Foundation of China (No. 21736007), the National Natural Science Foundation of China (Grant Nos. 21576178 and 21476155) and Research Project supported by Shanxi Scholarship Council of China (No. 2016-030).

Appendix A. Supplementary data

Supplementary data to this article can be found online at https://doi.org/10.1016/j.fuel.2021.122981.

References

[1] Luk HT, Mondelli C, Ferré DC, Stewart JA, Pérez-Ramírez J. Status and prospects in higher alcohols synthesis from syngas. Chem Soc Rev 2017;46(5):1358–426.
[2] Haider MA, Gogate MR, Davis RJ. Fe-promotion of supported Rh catalysts for direct conversion of syngas to ethanol. J Catal 2009;261(1):9–16.
[3] Wang J, Zhang Q, Wang Y. Rh-catalyzed syngas conversion to ethanol: Studies on the promoting effect of FeOx. Catal Today 2011;171(1):257–65.
[4] Li Z, Liu J, Zhao Y, Waterhouse GI, Chen GB, Shi R, Zhang X, Liu YM, Wen XD, Wu LZ, Tung CH, Zhang TR. Co-based catalysts derived from layered-double-hydroxide nanosheets for the photothermal production of light Olefins. Adv Mater 2018;30(31):1800527.
[5] Xiang Y, Barbosa R, Li X, Kruse N. Ternary cobalt–copper–niobium catalysts for the selective CO hydrogenation to higher alcohols. ACS Catal 2015;5(5):2929–34.
[6] Sun J, Wan S, Wang F, Lin J, Wang Y. Selective synthesis of methanol and higher alcohols over Cs/Cu/ZnO/Al2O3 catalysts. Ind Eng Chem Res 2015;54(32):7841–51.
[7] Cheng Z, Huang S, Li Y, Cai K, Yao D, Lv J, Wang SP, Ma XB. Carbonylation of dimethyl ether over MOR and Cu/H-MOR catalysts: comparative investigation of deactivation behavior. Appl Catal A 2019;576:1–10.
[8] Lv MM, Xie W, Sun S, Wu GM, Zheng LR, Chu SQ, Gao C, Bao J. Activated-carbon-supported K-Co–Mo catalysts for synthesis of higher alcohols from syngas. Catal Sci Technol 2015;5(5):2925–34.
[9] Liakakou ET, Heracleous E, Triantafyllidis KS, Lemonidou AA. K-promoted NiMo catalysts supported on activated carbon for the hydrogenation reaction of CO to higher alcohols: effect of support and active metal. Appl Catal B 2015;165:296–305.
[10] Fang KG, Li DB, Lin MG, Xiang ML, Wei W, Sun YH. A short review of heterogeneous catalytic process for mixed alcohols synthesis via syngas. Catal Today 2009;147(2):133–8.
[11] Anderson JA, Rochester CH, Wang Z. IR study of CO adsorption on Cu–Rh/SiO2 catalysts, coked by reaction with methane. J Mol Catal A: Chem 1999;139(2–3):285–303.
[12] Gonzalez S, Sousa C, Illas F. Features and catalytic properties of RhCu: a review. Int J Mod Phys B 2010;24(25n26):5128–38.
[13] Climent MJ, Corma A, Iborra S, Sabater MJ. Heterogeneous catalysis for tandem reactions. ACS Catal 2014;4(3):870–91.
[14] Ge X, Sun H, Dong K, Tao YQ, Wang Q, Chen YZ, Wang Y, Zhang QH. Copper–cobalt catalysts supported on mechanically mixed HZSM-5 and γ-Al2O3 for higher alcohols synthesis via carbon monoxide hydrogenation. RSC Adv 2019;9(26):14592–8.
[15] Kang J, He S, Zhou W, Shen Z, Li YY, Chen MS, Zhang QH, Wang Y. Single-pass transformation of syngas into ethanol with high selectivity by triple tandem catalysis. Nat Commun 2020;11(1):1–11.
[16] Cheng K, Gu B, Liu X, Kang J, Zhang Q, Wang Y. Direct and highly selective conversion of synthesis gas into lower olefins: design of a bifunctional catalyst combining methanol synthesis and carbon–carbon coupling. Angew Chem 2016;128(15):4803–6.
[17] Gao X, Xu B, Yang G, Feng X, Yoneyama Y, Taka U, Tsubaki N. Designing a novel dual bed reactor to realize efficient ethanol synthesis from dimethyl ether and syngas. Catal Sci Technol 2018;8(8):2087–97.

[18] Li X, San X, Zhang Y, Ichii T, Meng M, Tan Y, Tsubaki N. Direct synthesis of ethanol from dimethyl ether and syngas over combined H-mordenite and Cu/ZnO catalysts. ChemSusChem 2010;3(10):1192–9.
[19] Jiao F, Li JJ, Pan XL, Xiao J, Li HB, Ma H, Wei MM, Pan Y, et al. Selective conversion of syngas to light olefins. Science 2016;351(6277):1065–8.
[20] Liu XL, Zhou W, Yang YD, Cheng K, Kang JC, Zhang L, Zhang GQ, Min XJ, Zhang QH, Wang Y. Design of efficient bifunctional catalysts for direct conversion of syngas into lower olefins via methanol/dimethyl ether intermediates. Chem Sci 2018;9(20):4708–18.
[21] Li X, San X, Zhang Y, Ichii T, Meng M, Tan Y, Tsubaki N. Direct synthesis of ethanol from dimethyl ether and syngas over combined H-mordenite and Cu/ZnO catalysts. ChemSusChem 2010;3(10):1192–9.
[22] Kang JK, He S, Zhou W, Shen Z, Li YY, Chen MS, Zhang QH, Wang Y. Single-pass transformation of syngas into ethanol with high selectivity by triple tandem catalysis. Nat Commun 2020;11(1):1–11.
[23] Yang G, Tsubaki N, Shamoto J, Yoneyama Y, Zhang Y. Confinement effect and synergistic function of H-ZSM-5/Cu-ZnO-Al2O3 capsule catalyst for one-step controlled synthesis. J Am Chem Soc 2010;132(23):8129–36.
[24] Rizo R, Roldan Cuenya B. Shape-controlled nanoparticles as anodic catalysts in low-temperature fuel cells. ACS Energy Lett 2019;4(6):1484–95.
[25] Sun XC, Zhang RG, Wang BJ. Insights into the preference of CHx (x=1–3) formation from CO hydrogenation on Cu (111) surface. Appl Surf Sci 2013;265:720–30.
[26] Zheng HY, Zhang RG, Li Z, Wang BJ. Insight into the mechanism and possibility of ethanol formation from syngas on Cu(100) surface. J Mol Catal A: Chem 2015;404:115–30.
[27] Zhang DF, Zhang H, Guo L, Zheng K, Han XD, Zhang Z. Delicate control of crystallographic facet-oriented Cu2O nanocrystals and the correlated adsorption ability. J Mater Chem 2009;19(29):5220–5.
[28] Hua Q, Cao T, Gu XK, Lu JQ, Jiang ZQ, Pan XR, Luo LF, Li WX, Huang WX. Crystal-plane-controlled selectivity of Cu2O catalysts in propylene oxidation with molecular oxygen. Angew Chem 2014;126(19):4956–61.
[29] Sun S, Kong C, You H, Song X, Ding B, Yang Z. Facet-selective growth of Cu–Cu2O heterogeneous architectures. CrystEngComm 2014;14(1):40–3.
[30] Zhang Z, Wang SS, Song R, Cao T, Luo L, Chen XY, Gao YX, Lu JQ, Li WX, Huang WX. The most active Cu facet for low-temperature water gas shift reaction. Nat Commun 2017;8(1):1–10.
[31] Hua Q, Cao T, Gu XK, Lu J, Jiang Z, Pan XR, Luo LF, Li WX, Huang WX. Crystal-plane-controlled selectivity of Cu2O catalysts in propylene oxidation with molecular oxygen. Angew Chem 2014;126(19):4956–61.
[32] Xu F, Mudiyanselage K, Baber AE, Soldemo M, Weissenrieder J, White MG, Stacchiola DJ. Redox-mediated reconstruction of copper during carbon monoxide oxidation. J Phys Chem C 2014;118(29):15902–9.
[33] Wadayama T, Kubo K, Yamashita T, Tanabe T, Hatta A. Infrared reflection absorption study of carbon monoxide adsorbed on submonolayer Fe-covered Cu (100), (110), and (111) bimetallic surfaces. J Phys Chem B 2003;107:3768–73.
[34] Hayden BE, Kretzschmar K, Bradshaw AM. An infrared spectroscopic study of CO on Cu (111): the linear, bridging and physisorbed species. Surf Sci 1985;155:553–66.
[35] Poels EK, Brands DS. Modification of Cu/ZnO/SiO2 catalysts by high temperature reduction. Appl Catal A 2000;191(1–2):83–96.
[36] Gong JL, Yue HR, Zhao YJ, Zhao S, Zhao L, Lv J, Wang SP, Ma XB. Synthesis of ethanol via syngas on Cu/SiO2 catalysts with balanced Cu0–Cu+ sites. J Am Chem Soc 2012;134(34):13922–5.
[37] Yang C, Garl CW. Infrared studies of carbon monoxide chemisorbed on rhodium. J Phys Chem 1957;61(11):1504–12.
[38] Gao J, Mo X, Chien ACY, Torres W, Goodwin Jr JG. CO hydrogenation on lanthana and vanadia doubly promoted Rh/SiO2 catalysts. J Catal 2009;262(1):119–26.
[39] Force C, Belzunegui JP, Sanz J, Martınez-Arias A, Soria J. Influence of precursor salt on metal particle formation in Rh/CeO2 catalysts. J Catal 2001;197(1):192–9.
[40] Li F, Ma HF, Zhang HT, Ying WY, Feng DY. Ethanol synthesis from syngas on Mn- and Fe-promoted Rh/γ-Al2O3. C R Chim 2014;17(11):1109–15.
[41] Xu DD, Zhang HT, Ma HF, Qian WX, Ying WY. Effect of Ce promoter on Rh-Fe/TiO2 catalysts for ethanol synthesis from syngas. Catal Commun 2017;98:90–3.
[42] Yang GH, San XG, Jiang N, Tanaka Y, Li XG, Jin Q, Tao K, Meng FZ, Tsubaki N. A new method of ethanol synthesis from dimethyl ether and syngas in a sequential dual bed reactor with the modified zeolite and Cu/ZnO catalysts. Catal Today 2011;164:425–8.
[43] Wang D, Yang GH, Ma QX, Yoneyama Y, Tan YS, Han YZ, Tsubaki N. Facile solid-state synthesis of Cu–Zn–O catalysts for novel ethanol synthesis from dimethyl ether (DME) and syngas (CO+ H2). Fuel 2013;109:54–60.